

High- Q Surface Light Emission from Active Parity-Time-Symmetric Gratings

Tahere Hemati¹, Yi Zou,^{2,*} and Binbin Weng^{1,†}

¹School of Electrical and Computer Engineering, University of Oklahoma, Norman Oklahoma 73019, USA

²School of Information Science and Technology, ShanghaiTech University, Shanghai 201201, China



(Received 20 December 2021; revised 21 February 2022; accepted 25 March 2022; published 12 April 2022)

This work presents a theoretical investigation of an active photonic grating of the parity-time- (PT) symmetric architecture. The analytical study of the free-space mode propagation from the grating structure indicates the unique bifurcation property due to the PT -symmetry modulation. It is shown that both the gain-loss contrast and the lattice constant parameters are critical factors to modulate the active photonic system in between the PT -symmetry to the symmetry-broken phases. Furthermore, numerical simulations via the rigorous coupled-wave analysis (RCWA) method discover the existence of a unique spectral singularity phenomenon in this PT grating structure, which corresponds to a nontrivial single mode and near-zero bandwidth photonic resonant emission. Also, the guiding procedure for fulfilling spectral singularity modes is found to be related to the unique formation of the scattering matrix applied in the PT -symmetric photonic gratings. This theoretical work takes a fresh look into the active PT -symmetric photonic gratings focusing on the discovery of nontrivial free-space emission modes, which could contribute to the development of high-performance surface-emitting semiconductor devices.

DOI: [10.1103/PhysRevApplied.17.044023](https://doi.org/10.1103/PhysRevApplied.17.044023)

I. INTRODUCTION

Photonic gratings as optical components operating at the subwavelength region can be considered the aspiration of modern nanophotonics concepts such as photonic crystals and metamaterials [1]. Its applications have been expanded broadly from telecommunications [2] and astronomy [3] to chemistry [4] and biosensing [5]. The unique properties of photonic gratings are associated with the spatial modulation of the refractive index (RI). By optimizing grating parameters, including the period, thickness, and fill factor, we can modulate the amplitude and phase of the incident wave for various light-manipulation purposes, including optical filters [6], reflectors [7,8], absorbers [9], and resonators [10,11].

More recently, by drawing the fundamental concepts in quantum physics [i.e., parity-time (PT) symmetry] [12] to the realm of optics and photonics, alternative photonic applications, such as unidirectional emission [13] and asymmetric diffraction [14], appeared from periodical structures, including photonic gratings. The simplest definition of a PT -symmetric system is a non-Hermitian system whose Hamiltonian remains invariant under parity ($p \rightarrow -p, x \rightarrow -x$) and time-reversal ($p \rightarrow -p, x \rightarrow x, i \rightarrow -i$) operators, where p , x , and i are momentum,

location, and imaginary unite, respectively [12]. It is indicated that to satisfy this condition, the related potential should be $\hat{V}(x) = \hat{V}^*(-x)$. The equivalent condition for a optical system is $n(x) = n^*(-x)$ [15].

In practice, two geometrically identical coupled waveguides, one showing loss and the other one indicating the same amount of gain, can be the simplest example of an optical PT -symmetric system [15]. In this system, by increasing the gain (loss) coupling contrast between these two waveguides, the system transits from a PT -symmetric regime where all eigenvalues are real into a PT -symmetry broken regime where the eigenvalues are complex. Such a PT -symmetry broken phase shows extraordinary properties such as single-mode lasing [16]. In addition, there is also a transient point between these two regimes named exceptional point (EP). Both eigenvalues and eigenstates coalesce at EP [17], which has led to an enhanced sensitivity, resulting in supersensitive detectors [18,19]. The uniqueness of a PT -symmetric system lies in the beneficial role of optical loss, while in trivial systems, loss always has a destructive effect and it should be eliminated.

Over the past few years, scholars found that using more complicated optical platforms to realize the PT -symmetry concept can introduce nontrivial outcomes. For instance, one-dimensional bilayer heterostructures [20] could mix the PT -symmetry and PT -broken phase leading to a selective manipulation of electromagnetic radiation. Another example is the asymmetrical propagation of picosecond

*zouyi@shanghaitech.edu.cn

†binbinweng@ou.edu

pulses [21] enabled by the quasi-*PT* symmetry, which is useful for short-pulsed spectroscopy and optical communications applications. Moreover, leveraging *PT* symmetry in metasurfaces also enables more freedom to control the polarization of electromagnetic waves [22]. Furthermore, combining *PT* symmetry with other quantum concepts such as chirality has revealed more effects, including advanced polarization control, leading to chiral unidirectional lasers and wave isolators [23]. In addition, loss-induced transparency [24], nonreciprocal light propagation [25], unidirectional invisibility [13,26], and directional emission [27] are other unique properties of *PT*-symmetric systems that have been successfully revealed.

Among different photonic platforms for *PT*-symmetry studies, grating structures [28–31], have also attracted some special attention due to their unique light control properties. By far, reported studies have mostly focused on asymmetric diffraction [28], and unidirectional properties [32] based on passive grating designs. Herein, we instead investigate an “active” type of the *PT*-symmetric gratings and study the possible nontrivial phenomena besides the asymmetric diffraction effect. This research theoretically studies the emission properties of diffracted modes from an active grating by the Helmholtz equation, driving the related matrix and indicating symmetry, symmetry-broken, and exceptional-point regions. Moreover, numerically through the RCWA method, a nontrivial supernarrow emission is stimulated, and its resonating properties induced by *PT*-symmetric diffraction grating are discussed in detail.

II. THEORY AND ANALYTICAL SOLUTIONS

As just mentioned, the guiding procedure in gratings lies in the spatial RI modulation. On the other hand, to realize the *PT* symmetry, the RI modulation needs to satisfy $n(x) = n^*(-x)$. Therefore, the real part of RI modulation has to be a symmetric function, and its imaginary part should be an asymmetric function. Thus the RI modulation can be defined as

$$n(x) = n_0 + n \cos(2\pi x/a) + i\gamma \sin(2\pi x/a), \quad (1)$$

where a is the period, n_0 is the effective refractive index, and n and γ are the real and imaginary parts of the refractive index modulation, respectively.

Figure 1(a) shows the real (solid blue line) and imaginary (dashed red line) parts of the *PT*-symmetric refractive index distribution. The positive part of the imaginary RI indicates gain, and the negative part shows the induced loss. Figure 1(b) displays the real part of the RI modulation in two dimensions where the RI solely changes in the x direction, and the incident light is perpendicular to the periodicity. A_- , A_0 , and A_+ show the amplitude of the -1 , 0 , and $+1$ orders of diffracted grating modes, respectively.

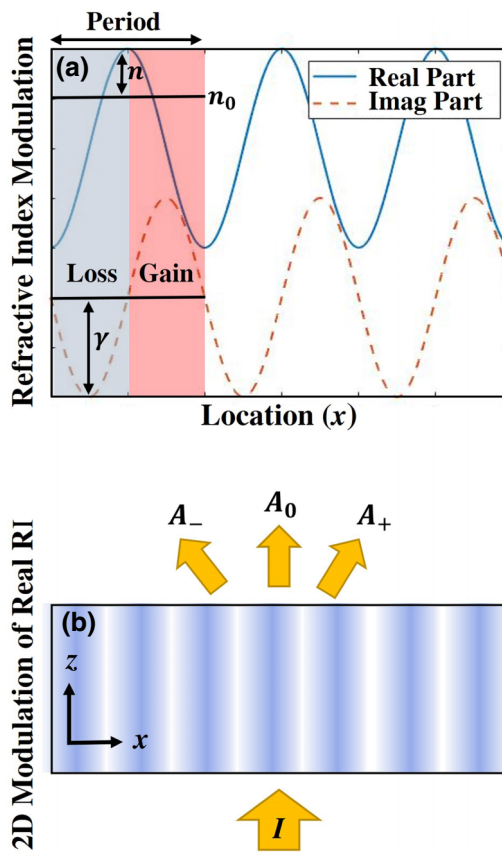


FIG. 1. (a) Real and imaginary parts of a *PT*-symmetric RI modulation in the x direction. (b) The real RI modulation in x and z direction.

Here, we study the wave propagation of an incident light entering along the z axis where the wave $E(x, z)$ obeys the Helmholtz equation [33,34]:

$$\nabla^2 E + k_0^2 n^2(x)E = 0, \quad (2)$$

in which $k_0 = 2\pi/\lambda$. Since the incident light is normal to the periodicity, both x and z components are effective. The general solution for $E(x, z)$ can be derived from Bloch's wave equation:

$$E(x, z) = u(x)e^{i\vec{\beta} \cdot \vec{r}}, \quad (3)$$

where $u(x)$ is a periodic function in the x direction

$$u(x) = \sum_{m=-\infty}^{\infty} A_m e^{-i2\pi mx/a}, \quad (4)$$

and in a two-dimensional (2D) plane

$$e^{i\vec{\beta} \cdot \vec{r}} = e^{i\beta_x x} e^{i\beta_z z}. \quad (5)$$

By substituting Eqs. (4) and (5) into Eq. (3):

$$E(x, z) = \sum_{m=-\infty}^{\infty} A_m e^{i\beta_z z} e^{i(\beta_x - 2\pi m/a)x}. \quad (6)$$

Considering the normal light incident, the wave number in x direction equals $2\pi m/a$, and consequently, the dispersion relation leads to

$$\beta_z = \sqrt{k_0^2 n_0^2 - (2\pi m/a)^2}. \quad (7)$$

If we consider the grating in a diffracted regime where $a >> \lambda$, β_z will be reduced to $\beta_z = k_0 n_0$. Thus, Eq. (6) can be rephrased as

$$E(x, z) = \sum_{m=-\infty}^{\infty} A_m e^{-i[mKx - k_0 n_0 z]}, \quad (8)$$

where A_m is the amplitude of the m _{th} diffracted mode, and $K = 2\pi/a$.

To analytically solve Eq. (2), in addition to $E(x, z)$ we need to find $n(x)$. Through Eq. (1), supposing n and γ are significantly smaller than n_0 , the RI modulation can be rephrased as

$$n(x) = \sqrt{n_0^2 + n_0 [c^+ e^{iKx} + c^- e^{-iKx}]}, \quad (9)$$

where $c^+ = n + \gamma$ and $c^- = n - \gamma$. Now, by substituting Eqs. (8) and (9) into Eq. (2), and considering the Raman-Nath approximation the wave-coupled equation [Eq. (10)] is obtained [29,35,36].

$$\frac{\partial A_m}{\partial z} + \frac{im^2 K^2 A_m}{2k_0 n_0} - \frac{ik_0}{2} [c^- A_{m+1} + c^+ A_{m-1}] = 0. \quad (10)$$

In contrast with Bragg gratings, in which only two first orders ($m = 0, 1$) at Bragg angle show nonzero amplitude, higher orders can indicate nonzero amplitude in thin gratings. However, in this active PT grating work with a normal incident light input, the amplitude of higher orders ($m = \pm 2$) are set to be significantly small [35]. Therefore, neglecting higher orders, which give us a reasonable approximation of the exact solution and provide a clear insight into the PT -symmetry concept [29]. Hence, Eq. (10) reduces to a set of coupled equations [Eq. (11)], which can also be written in a matrix form, shown in

Eq. (12).

$$\begin{aligned} \frac{\partial A_0}{\partial z} - \frac{ik_0}{2} [c^- A_{+1} + c^+ A_{-1}] &= 0, \\ \frac{\partial A_{+1}}{\partial z} + \frac{iK^2 A_{+1}}{2k_0 n_0} - \frac{ic^+ k_0 A_0}{2} &= 0, \\ \frac{\partial A_{-1}}{\partial z} + \frac{iK^2 A_{-1}}{2k_0 n_0} - \frac{ic^- k_0 A_0}{2} &= 0, \end{aligned} \quad (11)$$

$$\begin{aligned} M \begin{bmatrix} A_{+1} \\ A_0 \\ A_{-1} \end{bmatrix} &= \frac{i\partial}{\partial z} \begin{bmatrix} A_{+1} \\ A_0 \\ A_{-1} \end{bmatrix}, \\ M = \begin{bmatrix} \sigma & -k_0 c^+/2 & 0 \\ -k_0 c^-/2 & 0 & -k_0 c^+/2 \\ 0 & -k_0 c^-/2 & \sigma \end{bmatrix}, \end{aligned} \quad (12)$$

where $\sigma = K^2/2k_0 n_0$. To solve the equation, the eigenvalues are obtained as follows:

$$\lambda_1 = \sigma, \quad (13)$$

$$\lambda_2 = 1/2[\sigma + \sqrt{2k_0^2(n^2 - \gamma^2) + \sigma^2}], \quad (14)$$

$$\lambda_3 = 1/2[\sigma - \sqrt{2k_0^2(n^2 - \gamma^2) + \sigma^2}]. \quad (15)$$

While λ_1 is independent of the real and imaginary parts of the refractive index modulation, λ_2 and λ_3 are dependent on the real and imaginary parts. And once Eq. (16) is satisfied, the system will be located at its exceptional point, and λ_2 and λ_3 and their related eigenstates coalesce.

$$\gamma = \sqrt{n^2 + \frac{\sigma^2}{2k_0^2}}. \quad (16)$$

Further, once the imaginary part of the refractive index modulation is $\gamma > \sqrt{n^2 + \frac{\sigma^2}{2k_0^2}}$, the system enters into the symmetry-broken phase, indicating imaginary eigenvalues. Figures 2(a) and 2(b) show the real and imaginary parts of eigenvalues according to the imaginary part of the refractive index (γ), where the dashed blue line indicates λ_2 and the solid red line displays λ_3 . As we can see, in the symmetry region, both eigenvalues show a pure real value. However, immediately after the exceptional point, shown here by the dashed gray line, two eigenvalues bifurcates so that one of them possesses a negative imaginary part (λ_3) and the other one indicates a positive imaginary part (λ_2). It can be interpreted that one mode is trapped mostly in gain and the other one captured in loss and suppressed. The bifurcation is the most remarkable property of PT -symmetric systems [37,38]. This unique property is used in designing single-mode lasers [39,40], where undesired

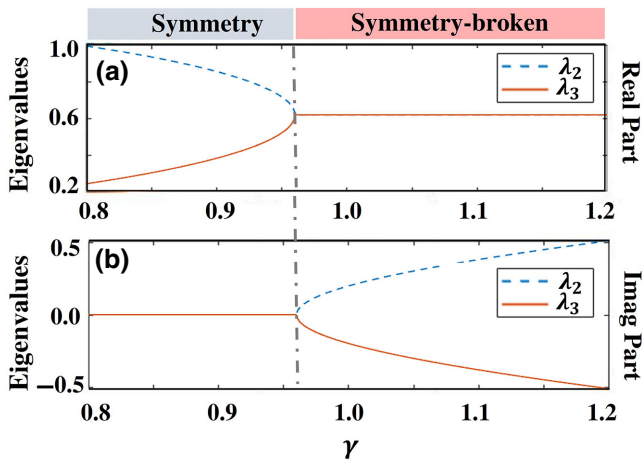


FIG. 2. (a) Real part and (b) imaginary part of eigenvalues according to the γ for a system with the periodicity of $2\text{ }\mu\text{m}$. The exceptional point is shown by the dashed gray line.

competing modes are captured in the loss and suppressed, and only confined modes in the gain are amplified.

In gratings that incident light is parallel to the periodicity [along x direction in Fig. 1(b)], only the ratio between real and imaginary parts of the refractive index (n and γ) determines the phase of the system [26]. However, in our designed grating, where the incident light is perpendicular to periodicity, the period plays an essential role.

Figures 3(a) and 3(b) show the real and imaginary parts of eigenvalues according to different period selections, respectively. This figure indicates that increasing the period will drive the system into the symmetry-broken phase. The dashed gray line shows the location of the exceptional point. As reflected from Eq. (16) in addition to real and imaginary parts of RI modulation, period and the effective refractive index can alter the system phase

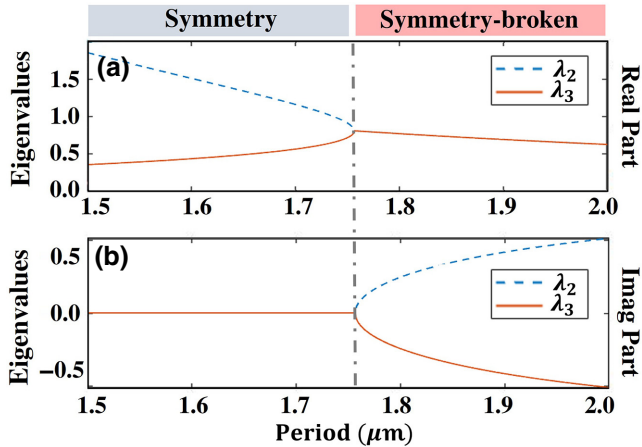


FIG. 3. (a) Real and (b) imaginary parts of eigenvalues according to the period for a PT -symmetric grating. The exceptional point is shown by the dashed gray line.

from symmetry to symmetry-broken phase. In other words, more design freedom exists in this unique active photonic grating platform.

This section analytically solves the Helmholtz equation for the dominant grating modes considering the Raman-Nath approximation. We show the impact of the imaginary part of RI modulation and period to shift the system from a PT -symmetry phase to the symmetry-broken stage. In the following section, we design a thin grating that follows the theory described above, and report the unique PT -symmetric photonic modes solved numerically by the RCWA method. Moreover, the related electric field and amplitude distribution over the grating is displayed, which extends the understanding of physical mechanisms leading to extraordinary phenomena observed in the active PT -symmetric photonic grating structures.

III. NUMERICAL SIMULATIONS

Figure 4 presents both a 3D schematic of the PT grating structure, where yellow and red parts show the gain and loss ($|\gamma|$), as well as its cross-section setup for conducting the numerical simulation study in this section. It is noted that, the $\text{In}_x\text{Ga}_{1-x}\text{As}$ material system is adopted for the design and study of the PT -symmetric grating effects, considering their large optical gain and loss tunability, and the well-established fabrication process for the dimensional accuracy control. Also, it has been the primary

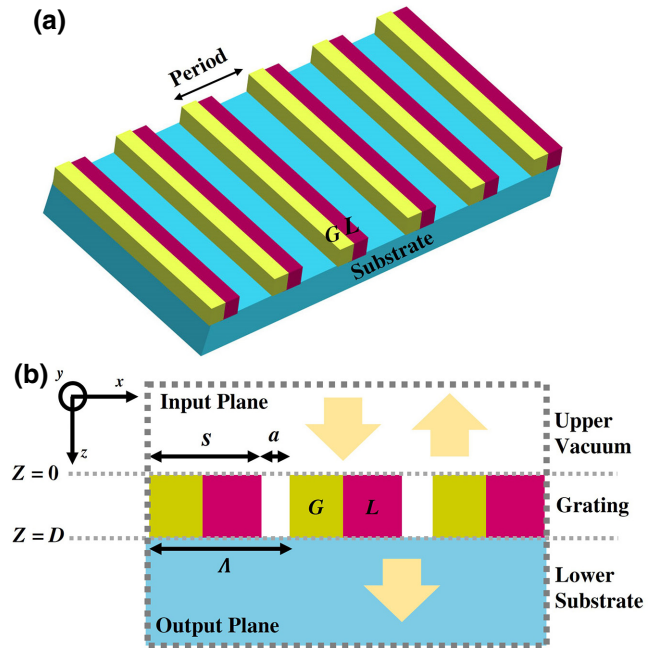


FIG. 4. (a) Three-dimensional (3D) schematic of the PT -symmetric gratings; (b) cross-section schematic of the grating, showing three divided regions: the upper-half vacuum region, the grating region, and the lower-half substrate region. Λ , a , and s are the grating period, gap, and bar width.

choice for studying *PT* photonics [40–42] in the near-infrared range. It is noted that conclusions to be made can also be applied to other material systems in other spectral domains. For example, antimony (Sb)-based III-V [43,44] and lead-chalcogenide materials [45–49] can be options for the mid-infrared active *PT* exploration.

One of the most well-known criteria of *PT*-symmetric systems is the spatial bifurcation of two modes in the symmetry-broken region. As presented in Fig. 2, in the symmetry-broken phase, two modes with the same real part of eigenvalues show the bifurcation, where one is captured mostly in the gain and the other trapped mainly in the loss. Thus, one mode is amplified while the other one is suppressed. This phenomenon is the primary mechanism behind the single-mode lasing in most of the *PT*-symmetric lasers. We expect that the numerical simulation demonstrates the same mechanism.

Figure 5 shows the spatial electric field distribution over a grating with the period of 1 μm and the thickness of 821 nm. The substrate and gain-loss areas are demonstrated in this figure, where *G* stands for gain and *L* stands for loss. The grating parameters are selected in a way that satisfies the Raman-Nath approximation criteria [Eq. (17)] that is implemented in the theoretical section

$$\begin{aligned} Q' \zeta &< 1 \\ Q' &= \frac{2\pi\lambda d}{n_0\Lambda^2 \cos\theta} \\ \zeta &= \frac{\pi nd}{2\lambda n_0}. \end{aligned} \quad (17)$$

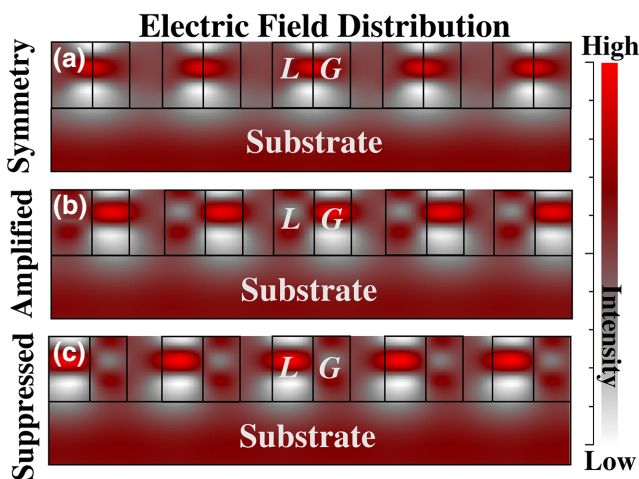


FIG. 5. Electric field distribution over the *PT*-symmetric grating where (a) $\gamma = 0.2$, associated with the symmetry phase. (b) $\gamma = 0.22$ associated with the symmetry-broken phase (amplified mode). (c) $\gamma = 0.22$ associated with the symmetry-broken phase (suppressed mode).

In Eq. (17), λ is the free-space wavelength, d is the grating thickness, n_0 is the effective refractive index, Λ is the grating period, n is the real part of the RI modulation, and θ is the incident angle.

Figure 5(a) shows the symmetric distribution of the electric field over the gain and loss areas so that no mode experiences net amplification or suppression. This pattern can be associated with the *PT*-symmetry phase, where both eigenvalues are purely real. By increasing gain-loss (γ) from 0.2 to 0.22, the system is shifted to the symmetry-broken phase, where one mode is captured in the gain and experiences the amplification. Figure 5(b) displays this mechanism clearly. However, the other mode is trapped in the loss and is suppressed [Fig. 5(c)].

After indicating the bifurcation over the *PT*-symmetric diffraction grating, it is also found that the *PT* grating system can produce a nontrivial single-mode surface emission with a proper configuration of grating structure parameters and gain-loss contrast (γ). Figure 6 illustrates three surface-emitting spectra from the *PT* grating structure with the period of 1 μm , the fill factor of 0.55, the thickness of 800 nm. Figure 4(b) shows the setup of our simulation model that includes three regions: the upper vacuum region, the middle grating region, and the lower substrate region. Considering the thicknesses of the upper and lower layers are generally multiorders of magnitude higher than the one of the middle grating layer, both of these two layers are set to be semi-infinite in our simulation. In addition, since the simulation path follows the input plane towards the output plane as indicated in Fig. 4(b), the upper vacuum space and lower substrate are also defined as the

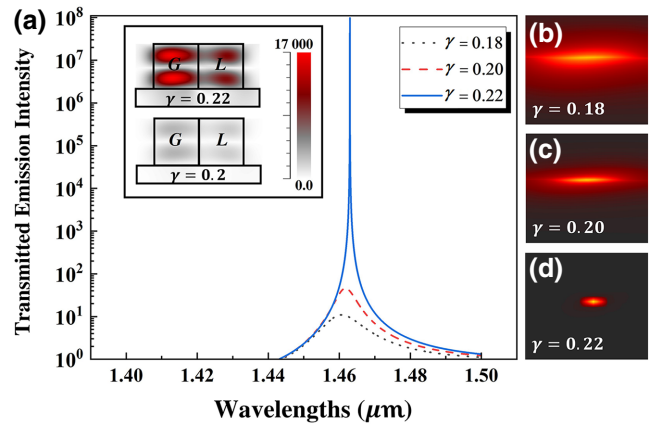


FIG. 6. (a) Logarithm form of the total transmitted spectra over wavelengths from the grating with $\gamma = 0.18$ (the black dotted line), $\gamma = 0.2$ (the red dashed line), and $\gamma = 0.22$ (the solid blue line). The amplitude distribution of the spectrum with $\gamma = 0.2$ and $\gamma = 0.22$ is displayed over one grating period in the inset. The transmitted emission coefficient map over wavelengths where γ changes from 0 to (b) 0.18, (c) 0.2, and (d) 0.22.

reflection and transmission regions. As such, the spectra in Fig. 6 are also noted as the transmitted emission spectra because they are observed from the substrate end ($Z = D$).

It should be pointed out that a similar single-mode PT emission can also be observed from the upper vacuum region, while the contributions from the diffraction orders are different. It is known that the cutoff condition [50] to prohibit the propagation of the higher ± 1 orders diffraction is $\Lambda < \lambda_0/n$, where Λ , λ_0 , and n are period, free-space wavelength, and refractive index, respectively [40]. In the upper-half vacuum region where $n = 1$, the wavelength (i.e., near $1.46\ \mu\text{m}$) is higher than the grating period ($\Lambda = 1\ \mu\text{m}$), which makes the ± 1 orders evanescent. Therefore, the high- Q emission observed from the upper region is solely contributed by the ground diffraction order. In contrast, considering our semi-infinite substrate's $n = 1.47$ ($\epsilon > 2.1$), in the lower substrate region, these two higher orders are not evanescent and allowed to propagate. Thus, the transmitted emission spectra in Fig. 6 are the combined emission effects from both the ground $m = 0$ and allowed ± 1 orders.

To better understand the dynamic of this nontrivial PT emission, we compare the diffraction efficiency of the transmitted modes in the logarithm form, where $\gamma = 0.18$, $\gamma = 0.2$, and $\gamma = 0.22$. Figure 6(a) illustrates this comparison, where the solid blue line is related to the system with $\gamma = 0.22$, the dashed red line is associated with $\gamma = 0.2$, and the black dotted line is associated with $\gamma = 0.18$. The inset shows field amplitude distribution over a unit cell in a grating with $\gamma = 0.2$ and $\gamma = 0.22$. The magnitude of amplitude is displayed by the colored bar. Furthermore, Figs. 6(b), 6(c), and 6(d) show the 2D transmitted emission coefficient map over wavelengths, where γ changes from 0 to 0.18, 0.2, and 0.22, respectively. As we can see, the broadness of the mode decreases by increasing γ , which matches with the full-width half maximum of the spectrum in Fig. 6(a). The main reason for this significant difference is attributed to the intensity of the confined field in the gain area. The inset illustrates that the amplitude of the confined mode in the gain area for the grating with $\gamma = 0.22$ is almost 10^3 greater than the amplitude of the trapped mode in the gain for the same grating but with $\gamma = 0.2$. The physical mechanism for this extraordinary phenomenon has roots in the scattering theory in PT -symmetric systems and the concept of spectral singularity [51–53].

Grating structures can be regarded as a typical scattering system in which the light propagation properties can be mathematically defined by using the scattering matrix function \mathbf{S} . Here, Eq. (18) shows a general \mathbf{S} matrix (of dimension $n \times m$) that associates the amplitudes of incoming modes ($\phi_1 \cdots \phi_m$) to the amplitudes of corresponding

outgoing modes ($\eta_1 \cdots \eta_m$).

$$\mathbf{S} \begin{bmatrix} \phi_1 \\ \vdots \\ \phi_m \end{bmatrix} = \begin{bmatrix} \eta_1 \\ \vdots \\ \eta_m \end{bmatrix}. \quad (18)$$

To solve eigenvalues of the \mathbf{S} matrix, Eq. (19) should be satisfied, where \mathbf{I} is the identity matrix, and λ stands for the eigenvalues of the \mathbf{S} matrix. A required condition to define an \mathbf{S} matrix is the unitary condition ($|\det \mathbf{S}|=1$).

$$|\mathbf{S} - \lambda \mathbf{I}| = 0. \quad (19)$$

For passive structures with real frequencies, this unitary condition is only satisfied by having unimodular \mathbf{S} -matrix eigenvalues ($|\lambda_m|=1$) [54]. Applying the PT operator on \mathbf{S} matrix meets the unitary condition. However, in contrast with passive structures, the only way to meet the unitary condition in PT -symmetric systems is not having unimodular eigenvalues. In these systems, the unitary condition can be satisfied by pairs reciprocal moduli as well ($\lambda_m=1/\lambda_m^*$) [55]. The former possibility to satisfy the unitary condition is related to the PT symmetry (unimodular eigenvalues), and the latter way (reciprocal eigenvalues) is associated with the PT -symmetry broken phase.

In the PT -symmetry broken phase, there are points at which poles and zeros of the \mathbf{S} matrix intersect on the real axis [56,57]. This intersection makes λ_m approach zero or equivalently $1/\lambda_m^* = \infty$, while their product is still unity. In fact, such singular points are known as the spectral singularity, corresponding to an extraordinary amplitude enhancement of the transmitted emission modes. In this study, via optimizing the grating structure and the introduced optical gain-loss, the active photonic system reaches the vicinity of the spectral singularity, where its imaginary part of the complex frequency solution is almost zero [51,58,59]. Consequently, the nontrivial optical resonance raising from the active PT grating structure appears in the form of a high- Q -factor surface-emitting single mode.

Figure 7 indicates Q factors of the resonant mode ($1.463\ \mu\text{m}$) with different introduced gain-loss (γ) to the grating. The calculation is based on the finite-difference frequency-domain method [60]. A sharp enhancement is observed when γ touches 0.22. This figure shows that only at a specific gain-loss value, here $\gamma = 0.22$, spectral singularity can occur, and higher or lower values cannot satisfy the spectral singularity condition. This is matched with the theory that claims only at the spectral singularity point, where λ_m goes to zero while $1/\lambda_m^*$ goes to ∞ . And the giant transmitted emission enhancement is related to $1/\lambda_m^*$, where its amplitude approaches infinity. Additionally, we want to point out that, although such an ultra-high- Q mode ($> 10^7$) has been achieved by other passive

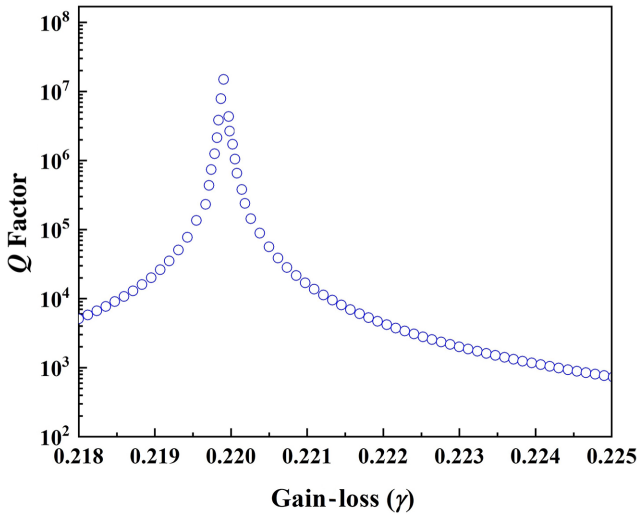


FIG. 7. Q factor of the resonance mode in the logarithm form with different introduced gain-loss (γ) to the grating.

structures, including whispering gallery cavities [61], and waveguide-coupled resonators [62,63], they all carry multilongitudinal modes and travel laterally in the same plane as their waveguides sit. The ultra-high- Q mode in our work is uniquely created from the active material and emits in the direction perpendicular to the gratings, which can lead to a pathway to develop the single-mode surface-emission laser devices. Moreover, in other mentioned works, the loss is considered an unwanted factor to be suppressed in order to achieve the high- Q performance. But here, due to the nontrivial properties of the PT -symmetry system, the loss becomes a beneficial role to provide fundamentally freedom to manipulate light and stimulate the high- Q emission.

IV. CONCLUSION

In this work, we report an alternative active grating platform with the optical gain and loss to realize nontrivial PT -symmetry modulation effects. Herein, by solving the Helmholtz equation in the Raman-Nath approximation, the bifurcation leading to confining the amplified mode in the gain region is indicated. We show that in the PT photonic grating structure, in addition to the gain-loss parameter, the period selection can also drive the system from PT -symmetry to the symmetry-broken phase. Moreover, a near zero-bandwidth photonic emission mode (i.e., at $1.463 \mu\text{m}$) can be stimulated and numerically demonstrated through the RCWA simulation. It is suggested that, by optimizing the optical gain-loss contrast, this nontrivial high- Q -factor resonance mode is the result of the photonic system's special spectral singularity effect, where one of the scattering states approaches zero while its reciprocal state approaches infinity. Considering the functionality of gratings in a broad

range of applications, we anticipate introducing active PT -symmetric gratings will offer alternative engineering strategies for developing high-performance surface-emitting lasers, and thus, advancing modern on-chip photonic applications.

ACKNOWLEDGMENTS

The authors would like to thank Dr. Mykola Kulishov for the insightful discussions. B.W. acknowledges partial support from OU's Big Idea Challenge award and the Oklahoma Center for the Advancement of Science and Technology's Research Grant No. AR21-052. Y.Z. acknowledges partial support from the Natural Science Foundation of Shanghai (Grant No. 21ZR1443100) and the National Natural Science Foundation of China (Grant No. 61705099).

- [1] N. Bonod and J. Neauport, Diffraction gratings: From principles to applications in high-intensity lasers, *Adv. Opt. Photonics* **8**, 156 (2016).
- [2] D. Milner, K. Didona, and D. Bannon, in *Optical Components and Materials II*, (International Society for Optics and Photonics, 2005), Vol. 5723, p. 34.
- [3] S. C. Barden, J. A. Arns, and W. S. Colburn, in *Optical Astronomical Instrumentation*, (International Society for Optics and Photonics, 1998), Vol. 3355, p. 866.
- [4] G. Ye, X. Li, and X. Wang, Diffraction grating of hydrogel functionalized with glucose oxidase for glucose detection, *Chem. Commun.* **46**, 3872 (2010).
- [5] A. W. Wark, H. J. Lee, A. J. Qavi, and R. M. Corn, Nanoparticle-enhanced diffraction gratings for ultrasensitive surface plasmon biosensing, *Anal. Chem.* **79**, 6697 (2007).
- [6] I. Nishi, T. Oguchi, and K. Kato, Broad-passband-width optical filter for multi/demultiplexer using a diffraction grating and a retroreflector prism, *Electron. Lett.* **21**, 423 (1985).
- [7] G. Almuneau, M. Condé, O. Gauthier-Lafaye, V. Bardinal, and C. Fontaine, High reflectivity monolithic subwavelength diffraction grating with GaAs/AlO_x stack, *J. Opt.* **13**, 015505 (2010).
- [8] T. Hemati and B. Weng, Theoretical study of leaky-mode resonant gratings for improving the absorption efficiency of the uncooled mid-infrared photodetectors, *J. Appl. Phys.* **124**, 053105 (2018).
- [9] C. Shi, X. F. Zang, L. Chen, Y. Peng, B. Cai, G. R. Nash, and Y. M. Zhu, Compact broadband terahertz perfect absorber based on multi-interference and diffraction effects, *IEEE Trans. Terahertz Sci. Technol.* **6**, 40 (2015).
- [10] I. Kaminow, H. Weber, and E. Chandross, Poly (methyl methacrylate) dye laser with internal diffraction grating resonator, *Appl. Phys. Lett.* **18**, 497 (1971).

- [11] T. Hemati and B. Weng, Theoretical design of coupled high contrast grating (CHCG) waveguides to enhance CO₂ light-absorption for gas sensing applications, *J. Appl. Phys.* **125**, 154502 (2019).
- [12] C. M. Bender and S. Boettcher, Real Spectra in non-Hermitian Hamiltonians Having PT-Symmetry, *Phys. Rev. Lett.* **80**, 5243 (1998).
- [13] L. Feng, Y. L. Xu, W. S. Fegadolli, M.-H. Lu, J. E. Oliveira, V. R. Almeida, Y.-F. Chen, and A. Scherer, Experimental demonstration of a unidirectional reflectionless parity-time metamaterial at optical frequencies, *Nat. Mater.* **12**, 108 (2013).
- [14] Y. Yang, H. Jia, Y. Bi, H. Zhao, and J. Yang, Experimental Demonstration of an Acoustic Asymmetric Diffraction Grating Based on Passive Parity-Time-Symmetric Medium, *Phys. Rev. Appl.* **12**, 034040 (2019).
- [15] C. E. Rüter, K. G. Makris, R. ElGanainy, D. N. Christodoulides, M. Segev, and D. Kip, Observation of parity-time symmetry in optics, *Nat. Phys.* **6**, 192 (2010).
- [16] M. A. Miri, P. LiKamWa, and D. N. Christodoulides, Large area single-mode parity-time-symmetric laser amplifiers, *Opt. Lett.* **37**, 764 (2012).
- [17] S. Özdemir, S. Rotter, F. Nori, and L. Yang, Parity-time symmetry and exceptional points in photonics, *Nat. Mater.* **18**, 783 (2019).
- [18] H. Hodaei, A. U. Hassan, S. Wittek, H. Garcia-Gracia, R. El-Ganainy, D. N. Christodoulides, and M. Khajavikhan, Enhanced sensitivity at higher-order exceptional points, *Nature* **548**, 187 (2017).
- [19] J. Wiersig, Enhancing the Sensitivity of Frequency and Energy Splitting Detection by Using Exceptional Points: Application to Microcavity Sensors for Single-Particle Detection, *Phys. Rev. Lett.* **112**, 203901 (2014).
- [20] E. Özgün, A. E. Serebryannikov, E. Özbay, and C. M. Soukoulis, Broadband mixing of PT-symmetric and PT-broken phases in photonic heterostructures with a one-dimensional loss/gain bilayer, *Sci. Rep.* **7**, 15504 (2017).
- [21] D. Tsvetkov, V. Bushuev, V. Konotop, and B. Mantsyzov, Broadband quasi-PT-symmetry sustained by inhomogeneous broadening of the spectral line, *Phys. Rev. A* **98**, 053844 (2018).
- [22] M. Lawrence, N. Xu, X. Zhang, L. Cong, J. Han, W. Zhang, and S. Zhang, Manifestation of PT Symmetry Breaking in Polarization Space with Terahertz Metasurfaces, *Phys. Rev. Lett.* **113**, 093901 (2014).
- [23] S. Droulias, I. Katsantonis, M. Kafesaki, C. M. Soukoulis, and E. N. Economou, Chiral Metamaterials with PT Symmetry and beyond, *Phys. Rev. Lett.* **122**, 213201 (2019).
- [24] A. Guo, G. Salamo, D. Duchesne, R. Morandotti, M. Volatier-Ravat, V. Aimez, G. Siviloglou, and D. Christodoulides, Observation of PT-Symmetry Breaking in Complex Optical Potentials, *Phys. Rev. Lett.* **103**, 093902 (2009).
- [25] H. Ramezani, T. Kottos, R. El-Ganainy, and D. N. Christodoulides, Unidirectional nonlinear PT-symmetric optical structures, *Phys. Rev. A* **82**, 043803 (2010).
- [26] Z. Lin, H. Ramezani, T. Eichelkraut, T. Kottos, H. Cao, and D. N. Christodoulides, Unidirectional Invisibility Induced by PT-symmetric Periodic Structures, *Phys. Rev. Lett.* **106**, 213901 (2011).
- [27] M. Kim, K. Kwon, J. Shim, Y. Jung, and K. Yu, Partially directional microdisk laser with two rayleigh scatterers, *Opt. Lett.* **39**, 2423 (2014).
- [28] X.-Y. Zhu, Y. L. Xu, Y. Zou, X.-C. Sun, C. He, M.-H. Lu, X.-P. Liu, and Y.-F. Chen, Asymmetric diffraction based on a passive parity-time grating, *Appl. Phys. Lett.* **109**, 111101 (2016).
- [29] F. Gao, Y. M. Liu, X. D. Tian, C. L. Cui, and J. H. Wu, Intrinsic link of asymmetric reflection and diffraction in non-hermitian gratings, *Opt. Express* **26**, 33818 (2018).
- [30] M. Kulishov and B. Kress, Free space diffraction on active gratings with balanced phase and gain/loss modulations, *Opt. Express* **20**, 29319 (2012).
- [31] M. Kulishov, H. Jones, and B. Kress, Analysis of PT-symmetric volume gratings beyond the paraxial approximation, *Opt. Express* **23**, 9347 (2015).
- [32] M. Kulishov, H. Jones, and B. Kress, Analysis of unidirectional non-paraxial invisibility of purely reflective PT-symmetric volume gratings, *Opt. Express* **23**, 18694 (2015).
- [33] T. K. Gaylord and M. Moharam, Analysis and applications of optical diffraction by gratings, *Proc. IEEE* **73**, 894 (1985).
- [34] T. Shui, W.-X. Yang, S. Liu, L. Li, and Z. Zhu, Asymmetric diffraction by atomic gratings with optical PT symmetry in the Raman-Nath regime, *Phys. Rev. A* **97**, 033819 (2018).
- [35] M. Berry and D. O'Dell, Diffraction by volume gratings with imaginary potentials, *J. Phys. A: Math. Gen.* **31**, 2093 (1998).
- [36] M. Berry, Lop-sided diffraction by absorbing crystals, *J. Phys. A: Math. Gen.* **31**, 3493 (1998).
- [37] L. Dong, C. Huang, and W. Qi, Symmetry breaking and restoration of symmetric solitons in partially parity-time-symmetric potentials, *Nonlinear Dyn.* **98**, 1701 (2019).
- [38] J. Yang, Symmetry breaking of solitons in one-dimensional parity-time-symmetric optical potentials, *Opt. Lett.* **39**, 5547 (2014).
- [39] B. Zhu, Q. J. Wang, and Y. D. Chong, Laser-mode bifurcations induced by PT-breaking exceptional points, *Phys. Rev. A* **99**, 033829 (2019).
- [40] L. Feng, Z. J. Wong, R. Ma, Y. Wang, and X. Zhang, Single-mode laser by parity-time symmetry breaking, *Science* **346**, 972 (2014).
- [41] W. E. Hayenga, H. Garcia-Gracia, E. S. Cristobal, M. Parto, H. Hodaei, P. LiKamWa, D. N. Christodoulides, and M. Khajavikhan, Electrically pumped microring parity-time-symmetric lasers, *Proc. IEEE* **108**, 827 (2019).
- [42] H. Hodaei, M. A. Miri, M. Heinrich, D. N. Christodoulides, and M. Khajavikhan, Parity-time-symmetric microring lasers, *Science* **346**, 975 (2014).
- [43] T. Hasenberg, R. Miles, A. Kost, and L. West, Recent advances in Sb-based midwave-infrared lasers, *IEEE J. Quantum Electron.* **33**, 1403 (1997).
- [44] M. Rattunde, J. Schmitz, C. Mermelstein, R. Kiefer, and J. Wagner, in *Mid-infrared semiconductor optoelectronics* (Springer, 2006), p. 131.
- [45] M. Eibelhuber, T. Schwarzl, G. Springholz, and W. Heiss, Lead salt microdisk lasers operating in continuous wave

- mode at $5.3 \mu\text{m}$ wavelength, *Appl. Phys. Lett.* **94**, 021118 (2009).
- [46] B. Weng, J. Ma, L. Wei, J. Xu, G. Bi, and Z. Shi, Mid-infrared surface-emitting photonic crystal microcavity light emitter on silicon, *Appl. Phys. Lett.* **97**, 231103 (2010).
- [47] B. Weng, J. Qiu, and Z. Shi, Continuous-wave mid-infrared photonic crystal light emitters at room temperature, *Appl. Phys. B* **123**, 29 (2017).
- [48] T. Hemati, X. Zhang, and B. Weng, A direct oriented-attachment growth of lead-chalcogenide mid-infrared nanocrystals film on amorphous substrates, *J. Mater. Chem. C* **8**, 13205 (2020).
- [49] T. Hemati, X. Zhang, and B. Weng, in *Smart Photonic and Optoelectronic Integrated Circuits XXII*, (International Society for Optics and Photonics, 2020), Vol. 11284, p. 1128418.
- [50] W. Hunter, Diffraction gratings and applications, by Erwin G. Loewen and Evgeny Popov, *Opt. Photonics News* **8**, 52 (1997).
- [51] A. Mostafazadeh, in *Geometric Methods in Physics* (Springer, 2015), p. 145.
- [52] L. Chaos-Cador and G. García-Calderón, Resonant states for complex potentials and spectral singularities, *Phys. Rev. A* **87**, 042114 (2013).
- [53] A. Mostafazadeh and H. Mehri-Dehnavi, Spectral singularities, biorthonormal systems and a two-parameter family of complex point interactions, *J. Phys. A: Math. Theor.* **42**, 125303 (2009).
- [54] C. Linton, Wave propagation. from electrons to photonic crystals and left-handed materials, by P. Markoš and CM Soukoulis: Scope: textbook. Level: final year undergraduates and first year postgraduates (2009).
- [55] Y. Chong, L. Ge, and A. D. Stone, PT-Symmetry Breaking and Laser-Absorber Modes in Optical Scattering Systems, *Phys. Rev. Lett.* **106**, 093902 (2011).
- [56] Y. Chong, L. Ge, H. Cao, and A. D. Stone, Coherent Perfect Absorbers: Time-Reversed Lasers, *Phys. Rev. Lett.* **105**, 053901 (2010).
- [57] D. G. Baranov, A. Krasnok, T. Shegai, A. Alù, and Y. Chong, Coherent perfect absorbers: Linear control of light with light, *Nat. Rev. Mater.* **2**, 17064 (2017).
- [58] A. Mostafazadeh, Resonance phenomenon related to spectral singularities, complex barrier potential, and resonating waveguides, *Phys. Rev. A* **80**, 032711 (2009).
- [59] A. Mostafazadeh, Optical spectral singularities as threshold resonances, *Phys. Rev. A* **83**, 045801 (2011).
- [60] S. C. Hagness and A. Taflove, Computational electrodynamics: The finite-difference time-domain method, Norwood, MA: Artech House (2000).
- [61] M. R. Foreman, J. D. Swaim, and F. Vollmer, Whispering gallery mode sensors, *Adv. Opt. Photonics* **7**, 168 (2015).
- [62] D. T. Spencer, J. F. Bauters, M. J. Heck, and J. E. Bowers, Integrated waveguide coupled Si_3N_4 resonators in the ultrahigh-Q regime, *Optica* **1**, 153 (2014).
- [63] X. Ji, F. A. Barbosa, S. P. Roberts, A. Dutt, J. Cardenas, Y. Okawachi, A. Bryant, A. L. Gaeta, and M. Lipson, Ultra-low-loss on-chip resonators with sub-milliwatt parametric oscillation threshold, *Optica* **4**, 619 (2017).